

Electromagnetically induced transparency with quantized fields in a dissipative optomechanical system

Sumei Huang ¹, Li Deng,² and Aixi Chen ^{1,*}

¹Key Laboratory of Optical Field Manipulation of Zhejiang Province, Department of Physics, Zhejiang Sci-Tech University, Hangzhou 310018, China

²School of Science, Zhejiang Sci-Tech University, Hangzhou 310018, China



(Received 11 September 2022; accepted 18 January 2023; published 26 January 2023)

We study electromagnetically induced transparency (EIT) using quantized fields in a dissipative optomechanical system with two mechanical oscillators coupled to each other via the Coulomb interaction. The weak probe field is a finite bandwidth squeezed vacuum field. In the absence of the Coulomb coupling, we show that an EIT dip is observable in the homodyne spectrum of the output field even for the squeezed vacuum field at the single-photon level. We find that the thermal environment has a negative impact on the EIT behavior. In the presence of the Coulomb coupling, we show that double EIT dips appear in the homodyne spectrum of the output field. The separation between the two EIT dips can be used to measure the Coulomb coupling strength. Compared to the case of the purely dissipative coupling, the combined dispersive and dissipative coupling can make the EIT dip broader and the minimum value of the EIT dip smaller.

DOI: [10.1103/PhysRevA.107.013524](https://doi.org/10.1103/PhysRevA.107.013524)

I. INTRODUCTION

The phenomenon of electromagnetically induced transparency (EIT) was first observed in a three-level atomic medium, in which the absorption of a weak coherent probe field could be vanished by applying a strong-coupling field to the atomic medium [1]. The EIT with a squeezed vacuum probe field in an atomic medium was also demonstrated experimentally [2,3]. The EIT with a squeezed vacuum plays an important role in storing and retrieving the squeezed vacuum [4,5].

The EIT effect was predicted theoretically [6] and demonstrated experimentally [7] in a dispersive optomechanical system, in which a mechanical oscillator is coupled to an optical field in the cavity via radiation pressure and the cavity resonance frequency is modified by the motion of the mechanical oscillator. The EIT in the dispersive optomechanical system has been applied for slow light [8], single-photon routers [9], light storage [10], and precise measurement of the electrical charge [11]. Later, the double EIT with two transparency windows was observed in different three-mode dispersive optomechanical systems, in which two mechanical oscillators are coupled to a common cavity field via radiation pressure [12], two coupled mechanical oscillators are coupled to a common cavity field via radiation pressure [13], a mechanical oscillator is coupled to a cavity field via radiation pressure and to a qubit via the Jaynes-Cummings interaction [14], and one mechanical oscillator is coupled to a cavity field via radiation pressure and to the other mechanical oscillator via the Coulomb interaction [15]. For the EIT with a weak

coherent probe field [6,7,12–15], the influence of the thermal noise of the mechanical oscillator on the EIT has not been considered. It has been shown that the EIT with quantized fields can be observed in a dispersive optomechanical system even in the presence of the mechanical thermal noise [16]. Moreover, the double EIT with quantized fields was observed in a dispersive optomechanical system where two mechanical oscillators are coupled via the Coulomb interaction and it was found that the double EIT can be used to measure the temperature of the environment [17].

The other kind of optomechanical coupling is the dissipative optomechanical coupling, which is characterized by the dependence of the cavity decay rate on the displacement of the mechanical oscillator [18]. The dissipative optomechanical system has recently attracted considerable attention as it was predicted that the dissipative optomechanical coupling offers the unique advantage of allowing the cooling of the mechanical oscillator in the unresolved-sideband regime [18–22]. Experimentally, the combination of the dispersive and dissipative coupling can cool a mechanical oscillator from room temperature to 126 mK [23] and the purely dissipative coupling can cool a mechanical oscillator from room temperature to 1.8 K [24]. Moreover, the dissipative optomechanical coupling has been realized in a number of optomechanical setups, such as a microdisk coupled to an oscillating waveguide [25], a Michelson-Sagnac interferometer with a movable membrane [23], a freestanding optical waveguide coupled to a whispering-gallery mode [24], a split-beam nanocavity [26], and a freestanding carbon nanotube coupled to an optical cavity [27]. In such a system, a variety of nonlinear phenomena have been explored, including high-precision detection [26,28–31], quadrature squeezed light [32–34], second-order correlation of the output light [33], quadrature squeezing

*Corresponding author: aixichen@zstu.edu.cn

of the mechanical oscillator [35–37], normal mode splitting [38,39], and the EIT effect [39]. In Ref. [39] it was shown that the EIT behavior with a weak coherent probe field in the dissipative optomechanical system is similar to the case of dispersive optomechanical coupling.

In this paper we investigate EIT with quantized fields in a dissipative optomechanical system with two mechanical oscillators which are mutually coupled via the Coulomb interaction. When the Coulomb coupling is absent, an EIT dip is observed at the line center of the homodyne spectrum of the output field by applying a strong-coupling field. We find that the temperature of the environment is detrimental to the EIT behavior. When the Coulomb coupling is present, two symmetric EIT dips are observed in the homodyne spectrum of the output field in the presence of a strong-coupling field. The spacing between the two EIT dips can be used to measure the Coulomb coupling strength. Compared to the purely dissipative coupling case, we show that the EIT dip becomes wider and its minimum value becomes smaller under the combined effects of dispersive and dissipative coupling.

The paper is structured as follows. In Sec. II the studied model is introduced and the equations of motion of the system operators are derived and solved in the steady state. In Sec. III the measurement of the output field is described and the analytical expression for the homodyne spectrum of the output field is given. In Sec. IV we discuss the homodyne spectrum of the output field in the absence of Coulomb coupling in the purely dissipative optomechanical system. In Sec. V we analyze the homodyne spectrum of the output field in the presence of Coulomb coupling in the purely dissipative optomechanical system. In Sec. VI we show the influence of the combined dispersive and dissipative optomechanical coupling on the EIT behavior in the homodyne spectrum of the output field in the absence and presence of the Coulomb coupling. In Sec. VII the main results of this work are summarized.

II. MODEL

The model to be considered is an optomechanical Michelson-Sagnac interferometer [23] with two mechanical oscillators (MO₁ and MO₂) separated by a distance r_0 , as shown in Fig. 1. One mechanical oscillator MO₁ is placed in the optical cavity and is interacting with the cavity field driven by a strong-coupling field at frequency ω_c . The other mechanical oscillator MO₂ is placed outside the cavity and is coupled to the mechanical oscillator MO₁ through the Coulomb interaction [15,17]. The mechanical oscillator MO₁ is partially transmitting. The two mechanical oscillators are approximated as damped harmonic oscillators with effective mass m_j , resonance frequency ω_j , and damping constant γ_j ($j = 1, 2$). Their displacement and momentum operators are denoted by q_1 and q_2 and by p_1 and p_2 , respectively. It has been demonstrated experimentally that the dispersive and dissipative couplings can take place between the cavity field and the mechanical oscillator MO₁ [23]. Thereby the cavity resonance frequency and the cavity decay rate can be changed by the motion of the mechanical oscillator MO₁, denoted by $\omega_0(q_1)$ and $\kappa(q_1)$, respectively. The Hamiltonian of the coupled system in a frame rotating at the coupling frequency

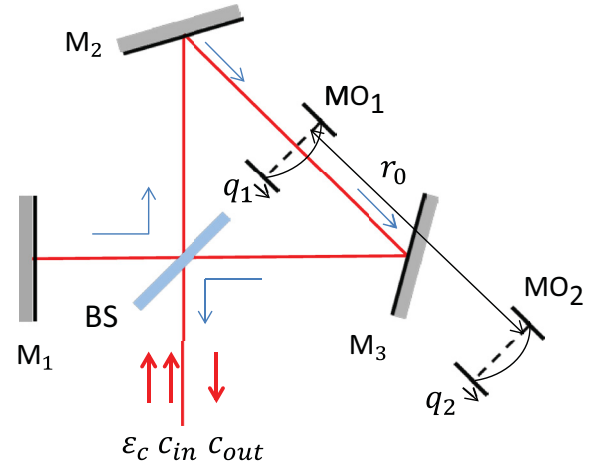


FIG. 1. Sketch of the Michelson-Sagnac interferometer formed by three fixed perfect reflecting mirrors (M₁, M₂, and M₃) and a fixed beam splitter (BS). The mechanical oscillator MO₁ is placed at the middle point between two mirrors M₂ and M₃. The two mechanical oscillators MO₁ and MO₂ are coupled via the Coulomb interaction, and the equilibrium distance between them is r_0 . A strong-coupling field with amplitude ε_c and a quantized field c_{in} are sent into the cavity. The output field from the cavity is c_{out} . Here q_1 and q_2 are the displacements of the two mechanical oscillators MO₁ and MO₂ from their respective equilibrium positions.

ω_c is given by

$$H = \hbar[\omega_0(q_1) - \omega_c]c^\dagger c + \frac{1}{2} \left(m_1 \omega_1^2 q_1^2 + \frac{p_1^2}{m_1} \right) + \frac{1}{2} \left(m_2 \omega_2^2 q_2^2 + \frac{p_2^2}{m_2} \right) + H_{12} + i\hbar\sqrt{2\kappa(q_1)}[c^\dagger(\varepsilon_c + c_{in}) - c(\varepsilon_c + c_{in}^\dagger)], \quad (1)$$

where the first term is the energy of the cavity field, c (c^\dagger) is the annihilation (creation) operator of the cavity field satisfying the Bose commutation relation $[c, c^\dagger] = 1$, the second and third terms are the energies of the two mechanical oscillators MO₁ and MO₂, respectively, the fourth term H_{12} represents the interaction energy between the two mechanical oscillators due to the Coulomb coupling, the last term describes the interactions of the cavity field with the coupling field and the quantum field c_{in} entering the beam splitter, and the amplitude ε_c of the coupling field can be calculated as $\varepsilon_c = \sqrt{\frac{\wp}{\hbar\omega_c}}$, with \wp the power of the coupling field. The incident quantized field c_{in} has a center frequency of $\omega_p = \omega_c + \omega_1$ and a finite bandwidth of Γ , which can be produced by a degenerate parametric amplifier [40]. The quantized field c_{in} has vanishing mean value $\langle c_{in} \rangle = 0$ and the frequency correlation functions [40]

$$\langle c_{in}(\omega)c_{in}(\Omega) \rangle = 2\pi \frac{M\Gamma^2}{\Gamma^2 + (\omega - \omega_1)^2} \delta(\omega + \Omega - 2\omega_1),$$

$$\langle c_{in}(\omega)c_{in}^\dagger(-\Omega) \rangle = 2\pi \left(\frac{N\Gamma^2}{\Gamma^2 + (\omega - \omega_1)^2} + 1 \right) \delta(\omega + \Omega), \quad (2)$$

where N is the mean number of photons in the squeezed vacuum field and M is the correlation between the two photons in the squeezed vacuum field. The parameters N and M satisfy the inequality $|M| \leq \sqrt{N(N+1)}$ [40–42]. For a pure squeezed vacuum field, the equality holds [40–42]. In this case, $N = \sinh^2 r$ and $M = |M|e^{i\phi} = \sqrt{N(N+1)}e^{i\phi}$, where r is the squeezing parameter and ϕ is the squeezing phase. The antinormally ordered correlation function has a broadband contribution coming from the incident vacuum noise. When $M = 0$, Eq. (2) describes a thermal field with the mean photon number $\frac{N\Gamma^2}{\Gamma^2 + (\omega - \omega_1)^2}$ around $\omega = \omega_1$, which is phase independent [41]. It has been shown that injecting a squeezed vacuum light into an optomechanical system can generate the squeezing of the mechanical oscillator [35,42] and enhance the sideband cooling of the mechanical oscillator [43].

It is assumed that the electrodes on the two mechanical oscillators MO₁ and MO₂ are charged by the bias gate voltages U_1 and $-U_2$, respectively. Thus the charges carried by the electrodes on the two mechanical oscillators MO₁ and MO₂ are C_1U_1 and $-C_2U_2$, respectively, where C_1 and C_2 are the capacitances of the bias gates on the two mechanical oscillators MO₁ and MO₂, respectively. Hence the interaction energy H_{12} is given by

$$H_{12} = \frac{-C_1U_1C_2U_2}{4\pi\epsilon_0|r_0 + q_1 - q_2|}, \quad (3)$$

where ϵ_0 is the permittivity of free space. When the displacements q_1 and q_2 of the two mechanical oscillators from their respective equilibrium positions are much smaller than the distance r_0 , the interaction energy H_{12} is approximated to second order in $\frac{q_1 - q_2}{r_0}$, which yields

$$H_{12} \approx \frac{-C_1U_1C_2U_2}{4\pi\epsilon_0r_0} \left(1 - \frac{q_1 - q_2}{r_0} + \frac{q_1^2}{r_0^2} + \frac{q_2^2}{r_0^2} - \frac{2q_1q_2}{r_0^2} \right), \quad (4)$$

where the first term is constant and does not affect the dynamics of the two mechanical oscillators; the second term is a linear term, which can be absorbed into the definition of the equilibrium positions of the two mechanical oscillators; the term proportional to q_1^2 (q_2^2) results in a shift in the mechanical frequency, which is much smaller than the bare mechanical frequency ω_1 (ω_2) and thus can be neglected; and the term proportional to q_1q_2 represents the coupling between the two mechanical oscillators. Thus the interaction energy H_{12} is given by

$$H_{12} = \hbar\lambda_0q_1q_2, \quad (5)$$

where $\lambda_0 = \frac{C_1U_1C_2U_2}{2\pi\hbar\epsilon_0r_0^2}$ is the Coulomb coupling strength [15,17,44,45] and can be adjusted by changing the charges carried by the two mechanical oscillators.

For a small displacement q_1 of the mechanical oscillator MO₁, the cavity resonance frequency $\omega_0(q_1)$ and the cavity decay rate $\kappa(q_1)$ can be approximated to first order in q_1 [23,25],

$$\begin{aligned} \omega_0(q_1) &\approx \omega_0 + \chi_0q_1, \\ \kappa(q_1) &\approx \kappa + g_0q_1, \end{aligned} \quad (6)$$

where ω_0 and κ are the cavity resonance frequency and the cavity decay rate for $q_1 = 0$, respectively, and χ_0 and g_0

represent the dispersive and dissipative coupling strengths between the cavity field and the mechanical oscillator MO₁, respectively. Similarly, $\sqrt{2\kappa(q_1)}$ can be approximated to first order in q_1 , $\sqrt{2\kappa(q_1)} \approx \sqrt{2\kappa}(1 + \frac{g_0}{2\kappa}q_1)$. The dimensionless displacement and momentum operators of the mechanical oscillators are represented by $Q_j = \sqrt{\frac{m_j\omega_j}{\hbar}}q_j$ and $P_j = \frac{p_j}{\sqrt{\hbar m_j\omega_j}}$, with $[Q_j, P_k] = i\delta_{jk}$ ($j, k = 1, 2$). The Hamiltonian of the system becomes

$$\begin{aligned} H &= \hbar(\omega_0 - \omega_c)c^\dagger c + \hbar\chi Q_1c^\dagger c + \frac{1}{2}\hbar\omega_1(Q_1^2 + P_1^2) \\ &+ \frac{1}{2}\hbar\omega_2(Q_2^2 + P_2^2) + \hbar\lambda Q_1Q_2 + i\hbar\sqrt{2\kappa}\left(1 + \frac{g}{2\kappa}Q_1\right) \\ &\times [c^\dagger(\epsilon_c + c_{\text{in}}) - c(\epsilon_c + c_{\text{in}}^\dagger)], \end{aligned} \quad (7)$$

where $\chi = \chi_0\sqrt{\frac{\hbar}{m_1\omega_1}}$, $g = g_0\sqrt{\frac{\hbar}{m_1\omega_1}}$, and $\lambda = \lambda_0\frac{\hbar}{\sqrt{m_1\omega_1 m_2\omega_2}}$.

The Heisenberg equations of motion for the system operators give

$$\begin{aligned} \dot{Q}_1 &= \omega_1P_1, \\ \dot{P}_1 &= -\chi c^\dagger c - \omega_1Q_1 - i\frac{g}{\sqrt{2\kappa}}[c^\dagger(\epsilon_c + c_{\text{in}}) - c(\epsilon_c + c_{\text{in}}^\dagger)] \\ &\quad - \lambda Q_2 - \gamma_1P_1 + \xi_1, \\ \dot{Q}_2 &= \omega_2P_2, \\ \dot{P}_2 &= -\omega_2Q_2 - \lambda Q_1 - \gamma_2P_2 + \xi_2, \\ \dot{c} &= -[\kappa + gQ_1 + i(\omega_0 - \omega_c + \chi Q_1)]c \\ &\quad + \sqrt{2\kappa}\left(1 + \frac{g}{2\kappa}Q_1\right)(\epsilon_c + c_{\text{in}}), \end{aligned} \quad (8)$$

where we have included the damping and noise terms. The ξ_1 (ξ_2) is the thermal Brownian noise arising from the thermal coupling of the mechanical oscillator MO₁ (MO₂) to its surrounding environment; they average to zero $\langle \xi_j \rangle = 0$ ($j = 1, 2$) and the frequency correlation functions

$$\langle \xi_j(\omega)\xi_k(\Omega) \rangle = 2\pi\delta_{jk}\gamma_j\frac{\omega}{\omega_j}\left[1 + \coth\left(\frac{\hbar\omega}{2k_B T}\right)\right]\delta(\omega + \Omega), \quad (9)$$

where k_B is the Boltzmann constant and T is the temperature of the mechanical oscillators' environment ($j, k = 1, 2$). The steady-state solutions of Eq. (8) can be obtained by setting all the time derivatives equal to zero, which are given by

$$\begin{aligned} P_{1s} &= 0, \\ Q_{1s} &= \frac{1}{\omega_1}\left(-\chi|c_s|^2 + i\frac{g}{\sqrt{2\kappa}}(c_s - c_s^*)\epsilon_c - \lambda Q_{2s}\right), \\ P_{2s} &= 0, \\ Q_{2s} &= -\frac{\lambda}{\omega_2}Q_{1s}, \\ c_s &= \frac{\mu\epsilon_c}{\kappa + gQ_{1s} + i\Delta}, \end{aligned} \quad (10)$$

where $\Delta = \omega_0 - \omega_c + \chi Q_{1s}$ is the effective cavity detuning, including the frequency shift induced by the dispersive optomechanical coupling, and $\mu = \sqrt{2\kappa}(1 + \frac{g}{2\kappa}Q_{1s})$. The Q_{1s}

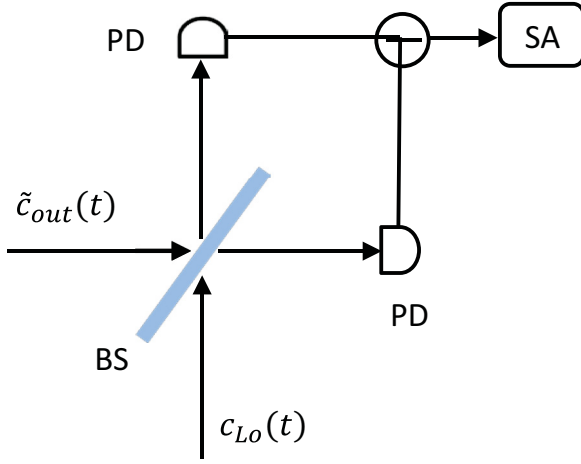


FIG. 2. Sketch of the homodyne measurement of the output field. The output field $\tilde{c}_{\text{out}}(t)$ and a strong local oscillator $c_{LO}(t)$ are combined through a lossless 50:50 beam splitter, where $\tilde{c}_{\text{out}}(t)$ is defined as the sum of the output field $c_{\text{out}}(t)$ from the cavity and the incident quantized field $c_{\text{in}}(t)$. Here PD denotes photodetector and SA spectrum analyzer.

and Q_{2s} are the steady-state displacements of the two mechanical oscillators MO_1 and MO_2 , respectively, and c_s is the steady-state amplitude of the cavity field. Note that Q_{1s} not only depends on c_s due to the dispersive and dissipative optomechanical couplings between the cavity field and the mechanical oscillator MO_1 , but also depends on Q_{2s} due to the Coulomb coupling between the two mechanical oscillators, Q_{2s} is dependent on Q_{1s} due to the Coulomb coupling between the two mechanical oscillators, and c_s is dependent on Q_{1s} due to the dissipative optomechanical coupling between the cavity field and the mechanical oscillator MO_1 .

III. THE OUTPUT FIELD AND ITS MEASUREMENT

The optical field exiting the cavity has many frequency components, whose frequencies in the original frame are $\omega_c \pm n\omega_1$ (n is integer). The incident quantized field is centered around $\omega_p = \omega_c + \omega_1$; thus we are interested in the component of the output field at the probe frequency ω_p . In order to detect the component of the output field at frequency ω_p , we consider a homodyne measurement scheme. The output field $\tilde{c}_{\text{out}}(t)$ is combined with an intense local oscillator $c_{LO}(t)$ at frequency ω_p on a 50:50 beam splitter, as indicated in Fig. 2. In a rotating frame at the frequency ω_c of the coupling field, $c_{LO}(t) = c_{LO}e^{-i\delta_0 t}$, where $\delta_0 = \omega_p - \omega_c$. The intensities of the two output fields of the beam splitter are measured by the two photodetectors, respectively. Then the difference between the two photocurrents of the two photodetectors is fed into the spectrum analyzer. When c_{LO} is real, the homodyne spectrum $X(\omega)$ of the output field provided by the spectrum analyzer is found to be

$$\begin{aligned} & \langle [c_{LO}^*(t)\tilde{c}_{\text{out}}(t) + \text{c.c.}][c_{LO}^*(t')\tilde{c}_{\text{out}}(t') + \text{c.c.}] \rangle \\ &= \frac{c_{LO}^2}{2\pi} \int d\omega e^{-i\omega(t-t')} X(\omega). \end{aligned} \quad (11)$$

In order to investigate the EIT phenomenon in the homodyne spectrum $X(\omega)$ of the output field, we need to find the fluctuation in the output field. The steady-state mean value of the output field makes no contribution to the homodyne spectrum $X(\omega)$ because it is at the frequency ω_c of the coupling field. For a strong-coupling field, the intracavity photon number $|c_s|^2$ is large, satisfying $|c_s|^2 \gg 1$. Thus it is reasonable to write the system operators in Eq. (8) as $Q_j = Q_{js} + \delta Q_j$, $P_j = P_{js} + \delta P_j$, ($j = 1, 2$), and $c = c_s + \delta c$, where the fluctuations δQ_j , δP_j , and δc are much smaller compared to the corresponding steady-state mean values Q_{js} , P_{js} , and c_s , respectively. Keeping the first order in the fluctuations, we obtain the quantum Langevin equations for the fluctuations

$$\begin{aligned} \delta \dot{Q}_1 &= \omega_1 \delta P_1, \\ \delta \dot{P}_1 &= \beta^* \delta c + \beta \delta c^\dagger - \omega_1 \delta Q_1 - \lambda \delta Q_2 - \gamma_1 \delta P_1 \\ &\quad + u^* c_{\text{in}} + u c_{\text{in}}^\dagger + \xi_1, \\ \delta \dot{Q}_2 &= \omega_2 \delta P_2, \\ \delta \dot{P}_2 &= -\omega_2 \delta Q_2 - \lambda \delta Q_1 - \gamma_2 \delta P_2 + \xi_2, \\ \delta \dot{c} &= -(\kappa + gQ_{1s} + i\Delta) \delta c + \alpha \delta Q_1 + \mu c_{\text{in}}, \end{aligned} \quad (12)$$

where $\alpha = g(\frac{\varepsilon_c}{\sqrt{2\kappa}} - c_s) - i\chi c_s$, $\beta = -(\chi c_s + i\frac{g}{\sqrt{2\kappa}} \varepsilon_c)$, and $u = i\frac{g}{\sqrt{2\kappa}} c_s$. Note that Eq. (12) is linear in the fluctuations. It can be solved by taking the Fourier transform to the frequency domain. We can find the displacement fluctuation $\delta Q_1(\omega)$ of the mechanical oscillator MO_1 and the fluctuation $\delta c(\omega)$ of the cavity field. The output field from the cavity is related to the cavity field via the input-output formalism $c_{\text{out}}(t) = \sqrt{2\kappa}(\bar{q}_1)c(t) - c_{\text{in}}(t)$ [46]; thus the fluctuation of the output field is found to be $\delta c_{\text{out}}(\omega) = \mu \delta c(\omega) + \frac{gc_s}{\sqrt{2\kappa}} \delta Q_1(\omega) - c_{\text{in}}(\omega)$. In order to study the absorption of the quantized probe field by the system, we define the output field as $\tilde{c}_{\text{out}}(t) = c_{\text{out}}(t) + c_{\text{in}}(t)$ and obtain the fluctuation of the output field

$$\begin{aligned} \delta \tilde{c}_{\text{out}}(\omega) &= E(\omega) c_{\text{in}}(\omega) + F(\omega) c_{\text{in}}^\dagger(-\omega) + V_1(\omega) \xi_1(\omega) \\ &\quad + V_2(\omega) \xi_2(\omega), \end{aligned} \quad (13)$$

where

$$\begin{aligned} E(\omega) &= \frac{gc_s}{\sqrt{2\kappa}} A_1(\omega) + \mu B_1(\omega), \\ F(\omega) &= \frac{gc_s}{\sqrt{2\kappa}} A_2(\omega) + \mu B_2(\omega), \\ V_1(\omega) &= \frac{gc_s}{\sqrt{2\kappa}} A_3(\omega) + \mu B_3(\omega), \\ V_2(\omega) &= \frac{gc_s}{\sqrt{2\kappa}} A_4(\omega) + \mu B_4(\omega), \end{aligned} \quad (14)$$

$A_1(\omega) = \frac{1}{d(\omega)} \omega_1 R_2(\omega) K^*(-\omega) [\beta^* \mu + K(\omega) u^*]$, $A_2(\omega) = \frac{1}{d(\omega)} \omega_1 R_2(\omega) K(\omega) [\beta \mu + K^*(-\omega) u]$, $A_3(\omega) = \frac{1}{d(\omega)} \omega_1 R_2(\omega) K(\omega) K^*(-\omega)$, $A_4(\omega) = -\frac{1}{d(\omega)} \lambda \omega_1 \omega_2 K(\omega) K^*(-\omega)$, $B_1(\omega) = \frac{1}{K(\omega)} [\alpha A_1(\omega) + \mu]$, $B_2(\omega) = \frac{1}{K(\omega)} \alpha A_2(\omega)$, $B_3(\omega) = \frac{1}{K(\omega)} \alpha A_3(\omega)$, $B_4(\omega) = \frac{1}{K(\omega)} \alpha A_4(\omega)$, $d(\omega) = R_2(\omega) [R_1(\omega) K(\omega) K^*(-\omega) - \omega_1 \beta^* K^*(-\omega) \alpha - \omega_1 \beta K(\omega) \alpha^*] - \lambda^2 \omega_1 \omega_2 K(\omega) K^*(-\omega)$, $R_1(\omega) = \omega_1^2 - \omega^2 - i\gamma_1 \omega$, $R_2(\omega) = \omega_2^2 - \omega^2 - i\gamma_2 \omega$, and $K(\omega) = \kappa + gQ_{1s} + i(\Delta - \omega)$. In Eq. (13) the first two terms are from the incident quantized field, in which the first term is at the probe frequency ω_p and the second term is

at the Stokes frequency $2\omega_c - \omega_p$ generated by the interaction between the coupling field and the mechanical oscillator MO_1 [16], and the last two terms are from the thermal noises of the two mechanical oscillators.

$$\begin{aligned}
X(\omega) = & E(\omega + \omega_1)E(-\omega + \omega_1)\frac{M\Gamma^2}{\Gamma^2 + \omega^2} + |E(\omega + \omega_1)|^2\frac{N\Gamma^2}{\Gamma^2 + \omega^2} + E^*(-\omega + \omega_1)E^*(\omega + \omega_1)\frac{M^*\Gamma^2}{\Gamma^2 + \omega^2} \\
& + |E(-\omega + \omega_1)|^2\frac{N\Gamma^2}{\Gamma^2 + \omega^2} + |E(\omega + \omega_1)|^2 + |F(-\omega + \omega_1)|^2 + |V_1(\omega + \omega_1)|^2\gamma_1\frac{\omega + \omega_1}{\omega_1}\left[1 + \coth\left(\frac{\hbar(\omega + \omega_1)}{2k_B T}\right)\right] \\
& + |V_1(-\omega + \omega_1)|^2\gamma_1\frac{\omega - \omega_1}{\omega_1}\left[1 + \coth\left(\frac{\hbar(\omega - \omega_1)}{2k_B T}\right)\right] + |V_2(\omega + \omega_1)|^2\gamma_2\frac{\omega + \omega_1}{\omega_2}\left[1 + \coth\left(\frac{\hbar(\omega + \omega_1)}{2k_B T}\right)\right] \\
& + |V_2(-\omega + \omega_1)|^2\gamma_2\frac{\omega - \omega_1}{\omega_2}\left[1 + \coth\left(\frac{\hbar(\omega - \omega_1)}{2k_B T}\right)\right], \tag{15}
\end{aligned}$$

where the first four terms with coefficient N or M are the contributions of the incident quantized field, the next two terms without coefficients N and M are the contributions of the incident vacuum noise, and the last four terms are the contributions of the thermal noises of the two mechanical oscillators. In the following numerical calculations, we use the parameters which are similar to those in the first experiment realizing the cooling of a mechanical oscillator through the combined dissipative and dispersive optomechanical coupling [23]: The wavelength of the coupling field $\lambda_c = \frac{2\pi c}{\omega_c} = 1064$ nm, the effective masses of the mechanical oscillators $m_1 = m_2 = 80$ ng, the resonance frequencies of the mechanical oscillators $\omega_1 = \omega_2 = \omega_m = 2\pi \times 136$ kHz, the quality factors of the mechanical oscillators $Q'_1 = Q'_2 = 5.8 \times 10^5$, and the damping rates of the mechanical oscillators $\gamma_1 = \omega_1/Q'_1 = \gamma_2 = \omega_2/Q'_2 = 2\pi \times 0.23$ Hz. The cavity decay rate is $\kappa = 0.05\omega_1 \ll \omega_1$; thus the system operates in the resolved-sideband regime. Moreover, the linewidth of the incident quantized field is $\Gamma = 2\kappa$ and the coupling field is tuned to the red mechanical sideband; thus the effective cavity detuning is $\Delta = \omega_1$. The other parameters are chosen appropriately so that the system is working in the stable regime.

IV. EIT IN THE HOMODYNE SPECTRUM $X(\omega)$ IN THE ABSENCE OF COULOMB COUPLING IN THE PURELY DISSIPATIVE OPTOMECHANICAL SYSTEM

If the position of the mechanical oscillator MO_1 and the reflectivity of the beam splitter in the optomechanical Michelson-Sagnac interferometer are chosen appropriately, only the dissipative optomechanical coupling exists in this system [19]. In this section we show how the power \wp of the coupling field, the parameters N and M of the incident quantized field, and the temperature T of the environment affect the homodyne spectrum $X(\omega)$ of the output field in the absence of the Coulomb coupling between the two mechanical oscillators in the purely dissipative optomechanical system. We choose the dissipative optomechanical coupling rate $g = -2\pi \times 0.1$ Hz [19,23]. Without the Coulomb coupling $\lambda = 0$, when the power of the coupling field is $\wp = 20$ μW , the steady-state displacement q_{1s} of the mechanical

oscillator MO_1 is found to be about -2.285×10^{-13} m, which is very small, and thus the approximation of $\kappa(q_1)$ in Eq. (6) is reasonable.

We first evaluate the homodyne spectrum $X(\omega)$ at $\omega = 0$, at which the EIT is expected in the presence of the coupling field. For a pure squeezed vacuum field with the squeezing phase $\phi = 0$ and large values of N , $N \approx M$, we obtain

$$\begin{aligned}
X(0) \approx & N[E(\omega_1) + E^*(\omega_1)]^2 + |E(\omega_1)|^2 + |F(\omega_1)|^2 \\
& + 2|V_1(\omega_1)|^2\gamma_1 \coth\left(\frac{\hbar\omega_1}{2k_B T}\right). \tag{16}
\end{aligned}$$

We assume that the power of the coupling field is $\wp = 20$ μW and the temperature of the environment is $T = 1$ mK. For $N = 10$ and $M = \sqrt{N(N+1)} \approx 10$, in Eq. (16), the first term $N[E(\omega_1) + E^*(\omega_1)]^2$ coming from the squeezed vacuum field is about 5.4×10^{-6} , which is close to 0, the sum of the next two terms arising from the incident vacuum noise is about 0.04, and the last term originating from the thermal noise of the mechanical oscillator MO_1 is about 0.16. In principle, the contribution of the squeezed vacuum field can be obtained by doing the experiment in the presence and absence of the squeezed vacuum field and by subtracting the results, i.e., $X(0) - X(0)|_{N=0}$. In some sense, the contribution of the squeezed vacuum field indicates perfect transparency at $\omega = 0$. For $N = 10$ and $M = 0$, the incident quantized field is phase independent. In this case, $X(0) = 2N|E(\omega_1)|^2 + |E(\omega_1)|^2 + |F(\omega_1)|^2 + 2|V_1(\omega_1)|^2\gamma_1 \coth(\frac{\hbar\omega_1}{2k_B T})$. In the expression of $X(0)$, the first term $2N|E(\omega_1)|^2$ coming from the incident quantized field is about 0.46 by using the above parameters. Thus the contribution of the incident quantized field does not exhibit perfect transparency at $\omega = 0$. For $N = 5$ and 10, the squeezing parameters of the squeezed vacuum field are found to be $r \approx 1.54$ and 1.87, respectively, and the degrees of squeezing of the squeezed vacuum field are $-10 \log_{10} e^{-2r} \approx 13.4$ and 16.2 dB, respectively. Currently, 15-dB squeezed vacuum states of light can be achieved experimentally [47]. In Fig. 3 the homodyne spectrum $X(\omega)$ of the output field is plotted as a function of the normalized frequency ω/ω_m in the absence and presence of the coupling field when $\lambda = 0$, $N = 5$, $M = \sqrt{N(N+1)}$ and 0, and $T = 1$ mK. We start with

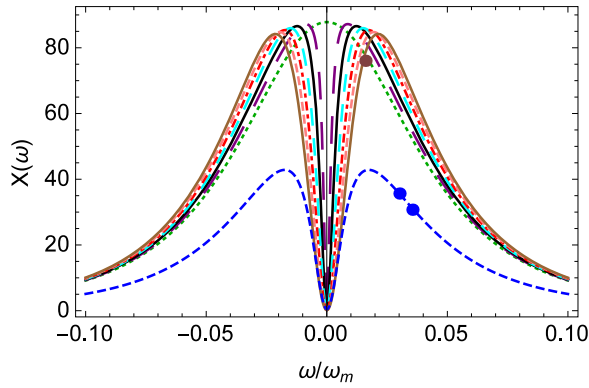


FIG. 3. Homodyne spectrum $X(\omega)$ as a function of the normalized frequency ω/ω_m in the absence (dotted curve) and presence of the coupling field with different powers when $\lambda = 0$, $N = 5$, $M = \sqrt{N(N+1)}$ and 0, and $T = 1$ mK. The long-dashed curve, solid curve, medium-dashed curve, dash-dotted curve, short-dashed curve, and solid curve with one circle marker are for $M = \sqrt{N(N+1)}$ and $\wp = 5, 10, 15, 20, 25$, and 30 μW , respectively, and the short-dashed curve with two circles is for $M = 0$ and $\wp = 20$ μW .

the case that the incident quantum field is phase dependent [$M = \sqrt{N(N+1)}$]. Without the coupling field ($\wp = 0$), it is seen that the homodyne spectrum $X(\omega)$ has a Lorentzian line profile centered at $\omega = 0$. In the presence of the coupling field ($\wp \neq 0$), the homodyne spectrum $X(\omega)$ exhibits an EIT window centered at $\omega = 0$. The reason is that the incident squeezed vacuum field at frequency ω_p destructively interferes with the quantum anti-Stokes field at frequency $\omega_c + \omega_1$ built up in the cavity due to the interaction between the strong-coupling field and the mechanical oscillator MO_1 . Moreover, the EIT window becomes wider if the power \wp of the coupling field increases, which is the same as that for the EIT with a weak coherent probe field in the dispersive optomechanical system [6,7] and in the dissipative optomechanical system [39]. For $\wp = 5, 10, 15, 20, 25$, and 30 μW , the linewidths of the EIT dips are about $0.003\omega_m, 0.006\omega_m, 0.009\omega_m, 0.012\omega_m, 0.014\omega_m$, and $0.017\omega_m$, respectively, and the minimum values of $X(\omega)$ at $\omega = 0$ are about 0.65, 0.34, 0.23, 0.18, 0.15, and 0.13, respectively. Hence the minimum value of $X(\omega)$ at $\omega = 0$ decreases with increasing power \wp of the coupling field. If the incident quantized field is phase independent ($M = 0$), it is found that the minimum value of $X(\omega)$ at $\omega = 0$ for $M = 0$ and $\wp = 20$ μW is about 0.43, which is larger than that for $M = \sqrt{N(N+1)}$ and $\wp = 20$ μW . The linewidth of the EIT dip is about $0.012\omega_m$, which is almost the same as that for $M = \sqrt{N(N+1)}$ and $\wp = 20$ μW . Moreover, we find that the depth of the EIT dip for $M = 0$ and $\wp = 20$ μW is about half that for $M = \sqrt{N(N+1)}$ and $\wp = 20$ μW . In Fig. 4 the homodyne spectrum $X(\omega)$ of the output field is plotted as a function of the normalized frequency ω/ω_m for different squeezing phases ϕ of the squeezed vacuum field when $\lambda = 0$, $N = 5$, $M = \sqrt{N(N+1)}e^{i\phi}$, $\wp = 10$ μW , and $T = 1$ mK. When the squeezing phase ϕ is increased from 0 to $5\pi/6$, it is seen that the homodyne spectrum $X(\omega)$ exhibits an EIT dip at $\omega = 0$. When $\phi = \pi$, the homodyne spectrum $X(\omega)$ does not exhibit an EIT dip at $\omega = 0$; instead, there is a small peak at $\omega = 0$ and the peak value of $X(\omega)$ at $\omega = 0$ is

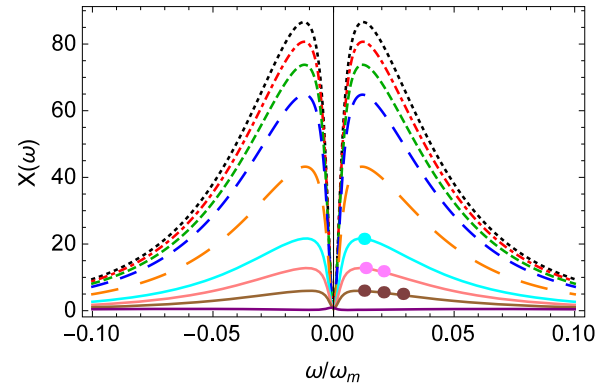


FIG. 4. Homodyne spectrum $X(\omega)$ as a function of the normalized frequency ω/ω_m for different squeezing phases ϕ of the squeezed vacuum field when $\lambda = 0$, $N = 5$, $M = \sqrt{N(N+1)}e^{i\phi}$, $\wp = 10$ μW , and $T = 1$ mK. The curves from top to bottom (dotted curve, dash-dotted curve, short-dashed curve, medium-dashed curve, long-dashed curve, solid curve with one circle, solid curve with two circles, solid curve with three circles, and solid curve) correspond to $\phi = 0, \pi/6, \pi/4, \pi/3, \pi/2, 2\pi/3, 3\pi/4, 5\pi/6$, and π , respectively.

about 0.84. For $\phi = 0, \pi/6, \pi/4, \pi/3, \pi/2, 2\pi/3, 3\pi/4$, and $5\pi/6$, the minimum values of $X(\omega)$ at $\omega = 0$ are about 0.34, 0.37, 0.41, 0.46, 0.59, 0.71, 0.76, and 0.81, respectively, and the linewidths of the EIT dips are approximately equal (about $0.006\omega_m$). Hence, increasing the squeezing phase ϕ from 0 to $5\pi/6$, the minimum value of $X(\omega)$ at $\omega = 0$ becomes larger, the linewidth of the EIT dip almost remains unchanged, and the depth of the EIT dip at $\omega = 0$ becomes smaller. Therefore, the EIT behavior is most pronounced when $\phi = 0$. For the remainder of the paper, we consider the cases of $M = \sqrt{N(N+1)}$ and 0.

Figure 5 plots the homodyne spectrum $X(\omega)$ of the output field versus the normalized frequency ω/ω_m in the absence and presence of the coupling field when $\lambda = 0$, $N = 1$ and 5, $M = \sqrt{N(N+1)}$ and 0, and $T = 10$ and 50 mK. First we consider the case of $M = \sqrt{N(N+1)}$. For a given temperature T , in the presence of the coupling field with the power $\wp = 20$ μW , it is seen that the EIT dip still exists in the homodyne spectrum $X(\omega)$ even if the mean photon number of the squeezed vacuum field is $N = 1$ and 5, the minimum values of the two EIT dips for $N = 1$ and 5 are almost the same (about 1.60 for $T = 10$ mK and about 7.91 for $T = 50$ mK), and the linewidths of the two EIT dips for $N = 1$ and 5 are almost the same (about $0.012\omega_m$). Comparing the curves for $\wp = 20$ μW , $N = 5$, and $M = \sqrt{N(N+1)}$ in Fig. 5 with those in Fig. 3, we note that the minimum value of the EIT dip increases with the rise of the temperature T and thus the temperature T of the environment has a negative effect on the EIT behavior. Additionally, the above numerical results for the EIT with the quantized field are similar to those for the EIT with the quantized field in the dispersive optomechanical system [16]. Next we look at the case of $M = 0$. For a given temperature T , with the coupling field ($\wp = 20$ μW), it is seen that the EIT dip still appears in the homodyne spectrum $X(\omega)$ when $N = 1$ and 5 and the linewidths of the two EIT dips for $N = 1$ and 5 are almost equal (about $0.012\omega_m$), which are almost the same as those in the case of $M = \sqrt{N(N+1)}$. When $T = 10$ mK,

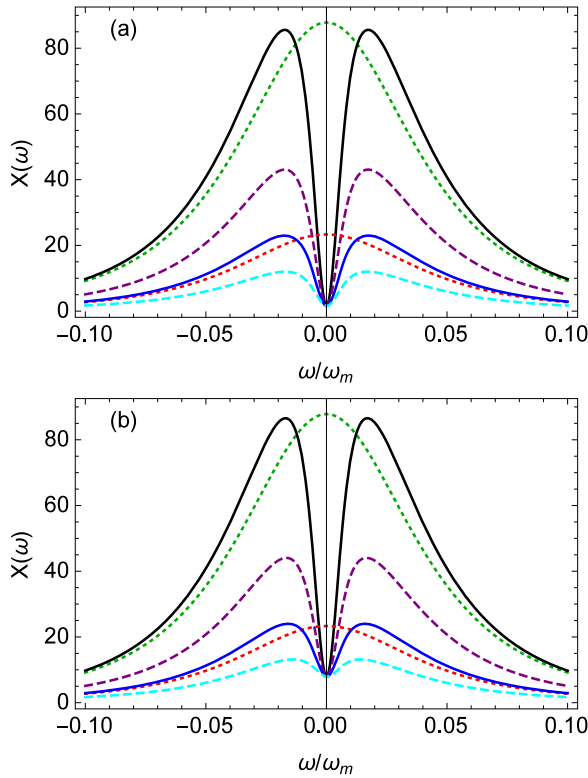


FIG. 5. Homodyne spectrum $X(\omega)$ as a function of the normalized frequency ω/ω_m for different values of the parameter N in the absence (dotted curves) and presence (solid and dashed curves) of the coupling field with the power $\wp = 20 \mu\text{W}$ when $\lambda = 0$, $M = \sqrt{N(N+1)}$ and 0, and (a) $T = 10 \text{ mK}$ and (b) $T = 50 \text{ mK}$. In each plot the upper three curves are for $N = 5$ and the lower three curves are for $N = 1$; the solid curves are for $M = \sqrt{N(N+1)}$ and the dashed curves are for $M = 0$.

the minimum values of the two EIT dips for $N = 1$ and 5 are about 1.67 and 1.85, respectively. When $T = 50 \text{ mK}$, the minimum values of the two EIT dips for $N = 1$ and 5 are about 7.97 and 8.16, respectively. Hence, for the given values of the parameters T and N , the minimum value of the EIT dip for $M = 0$ is larger than that for $M = \sqrt{N(N+1)}$. We compare the curves for $\wp = 20 \mu\text{W}$, $N = 5$, and $M = 0$ in Fig. 5 with those in Fig. 3 and find that the minimum value of the EIT dip becomes larger for a higher temperature T and thus the temperature T of the environment is detrimental to the EIT behavior. Note that the temperature $T = 10 \text{ mK}$ is reachable by current dilution refrigerators [48].

In the above analysis, the center frequency of the incident quantized field is $\omega_p = \omega_c + \omega_1$. If the incident quantized field is centered around $\omega_p = \omega_c + 2\omega_1$, the homodyne spectrum $X(\omega)$ of the output field in Eq. (11) still exhibits an EIT dip in the presence of the strong-coupling field, which is the result of the destructive interference between the incident quantized field at frequency $\omega_p = \omega_c + 2\omega_1$ and the second-order upper sideband generation at frequency $\omega_c + 2\omega_1$ generated by the interaction of the strong-coupling field with the mechanical oscillator MO_1 . In the resolved-sideband limit $\omega_1 \gg \kappa$, if the strong-coupling field is red detuned from the cavity resonance with $\Delta = \omega_1$, the intensity of the

second-order upper sideband generation at frequency $\omega_c + 2\omega_1$ is much smaller than the intensity of the quantum anti-Stokes field at frequency $\omega_c + \omega_1$ since the frequency $\omega_c + 2\omega_1$ of the second-order upper sideband generation is far away from the cavity resonance frequency ω_0 while the frequency $\omega_c + \omega_1$ of the quantum anti-Stokes field is close to cavity resonance frequency ω_0 . Therefore, the depth of the EIT dip in the homodyne spectrum $X(\omega)$ for the quantized probe field at frequency $\omega_p = \omega_c + 2\omega_1$ is much smaller than that for the quantized probe field at frequency $\omega_p = \omega_c + \omega_1$.

V. DOUBLE EIT IN THE HOMODYNE SPECTRUM $X(\omega)$ IN THE PRESENCE OF COULOMB COUPLING IN THE PURELY DISSIPATIVE OPTOMECHANICAL SYSTEM

In this section we discuss the effects of the Coulomb coupling strength λ , the parameters N and M of the incident quantized field, and the temperature T of the environment on the homodyne spectrum $X(\omega)$ of the output field in the presence of the Coulomb coupling between the two mechanical oscillators in the purely dissipative optomechanical system. The dissipative optomechanical coupling rate is still chosen to be $g = -2\pi \times 0.1 \text{ Hz}$ [19,23]. When the Coulomb coupling strength is $\lambda = \kappa$ and the power of the coupling field is $\wp = 20 \mu\text{W}$, the steady-state displacement q_{1s} of the mechanical oscillator MO_1 is about $-2.291 \times 10^{-13} \text{ m}$, which is very small, and thus the approximation of $\kappa(q_1)$ in Eq. (6) is valid. In Fig. 6 the homodyne spectrum $X(\omega)$ of the output field is plotted as a function of the normalized frequency ω/ω_m for different Coulomb coupling strengths λ in the presence of the coupling field when $N = 5$, $M = \sqrt{N(N+1)}$ and 0, $\wp = 10$ and $20 \mu\text{W}$, and $T = 1 \text{ mK}$. For the fixed values of the parameters \wp and M , in the absence of the Coulomb coupling ($\lambda = 0$), there is only a single EIT dip in the homodyne spectrum $X(\omega)$, which is the same as that in Fig. 3. For the fixed values of \wp and M , in the presence of the Coulomb coupling ($\lambda \neq 0$), it is seen that the two symmetric EIT dips appear in the homodyne spectrum $X(\omega)$. When $M = \sqrt{N(N+1)}$ or 0, the linewidths of the double EIT dips for $\lambda = 0.5\kappa$ and κ are almost identical (about $0.003\omega_m$ for $\wp = 10 \mu\text{W}$ and about $0.006\omega_m$ for $\wp = 20 \mu\text{W}$). When $M = \sqrt{N(N+1)}$, the minimum values of the double EIT dips for $\lambda = 0.5\kappa$ and κ are about 0.66 and 0.69 for $\wp = 10 \mu\text{W}$ and about 0.34 and 0.34 for $\wp = 20 \mu\text{W}$. When $M = 0$, the minimum values of the double EIT dips for $\lambda = 0.5\kappa$ and κ are about 0.69 and 1.19 for $\wp = 10 \mu\text{W}$, respectively, and about 0.46 and 0.35 for $\wp = 20 \mu\text{W}$, respectively. When $M = \sqrt{N(N+1)}$ or 0 and $\wp = 10$ or $20 \mu\text{W}$, the locations of the double EIT dips for $\lambda = 0.5\kappa$ and κ are at frequencies $\omega = \pm 0.0125\omega_m$ and $\pm 0.025\omega_m$, respectively. Hence, with increasing Coulomb coupling strength λ , the separation D between the two EIT dips becomes larger. The dependence of the separation D between the two EIT dips on the Coulomb coupling strength λ is shown in Fig. 7. It is seen that the separation D between the two EIT dips increases linearly with increasing Coulomb coupling strength λ . This result is the same as that for the double EIT with a weak coherent probe field in the dispersive optomechanical system with two mechanical oscillators coupled via the Coulomb interaction [15]. Thus it is possible to determine the Coulomb coupling strength λ between

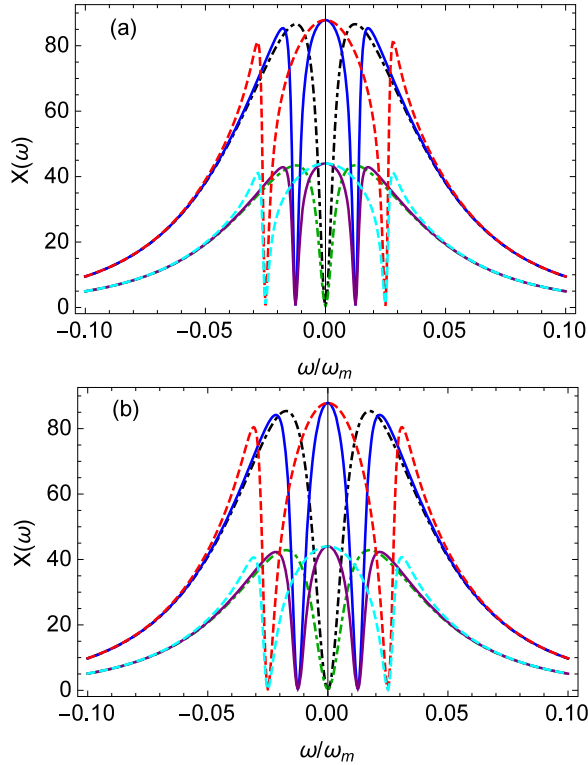


FIG. 6. Homodyne spectrum $X(\omega)$ as a function of the normalized frequency ω/ω_m for different Coulomb coupling strengths λ in the presence of the coupling field when $N = 5$, $M = \sqrt{N(N+1)}$ and 0 , $T = 1$ mK, and (a) $\varphi = 10$ μW and (b) $\varphi = 20$ μW . In each plot the upper three curves are for $M = \sqrt{N(N+1)}$ and the lower three curves are for $M = 0$; the dash-dotted, solid, and dashed curves represent $\lambda = 0, 0.5\kappa$, and κ , respectively.

the two mechanical oscillators from a measurement of the separation D between the two EIT dips in the homodyne spectrum $X(\omega)$. Note that the double EIT in the homodyne spectrum $X(\omega)$ is induced by the Coulomb coupling between the two mechanical oscillators with identical frequencies. This is different from the previous work [12], where the double EIT in a dispersive optomechanical system is generated by the frequency difference between the two mechanical oscillators.

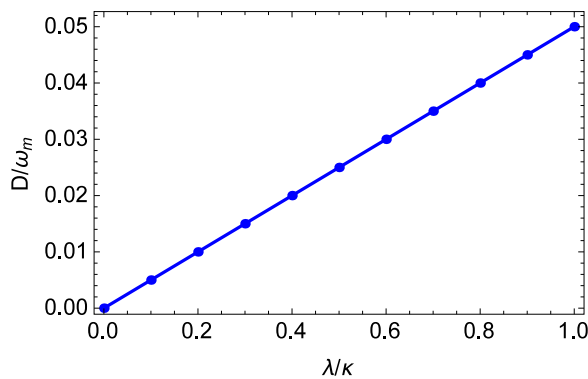


FIG. 7. Separation D between the two EIT dips as a function of the Coulomb coupling strength λ/κ when $N = 5$, $M = \sqrt{N(N+1)}$, $\varphi = 20$ μW , and $T = 1$ mK.

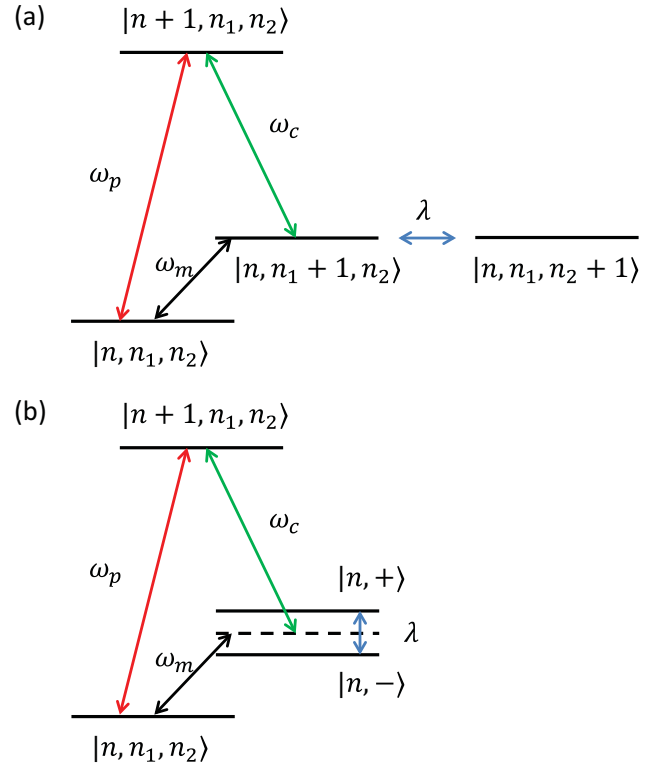


FIG. 8. (a) Energy-level diagram of the optomechanical system. Here $|n+1, n_1, n_2\rangle \leftrightarrow |n, n_1, n_2\rangle$ is the excitation at the cavity frequency ω_0 , $|n, n_1, n_2\rangle \leftrightarrow |n, n_1+1, n_2\rangle$ is the mechanical excitation at frequency ω_1 , the coupling field drives the transition $|n+1, n_1, n_2\rangle \leftrightarrow |n, n_1+1, n_2\rangle$, and the Coulomb coupling drives the transition $|n, n_1+1, n_2\rangle \leftrightarrow |n, n_1, n_2+1\rangle$, where n, n_1 , and n_2 are the intracavity photon number, the phonon number of the MO₁, and the phonon number of the MO₂, respectively. (b) Energy-level diagram of the optomechanical system in the dressed-state picture. Here $|n, \pm\rangle$ are the two dressed states generated by the Coulomb coupling, whose frequency difference is λ .

The double EIT phenomenon can be explained by the energy-level diagram of the system shown in Fig. 8. The Coulomb coupling between the two states $|n, n_1+1, n_2\rangle$ and $|n, n_1, n_2+1\rangle$ leads to the generation of the two dressed states $|n, \pm\rangle = \frac{1}{\sqrt{2}}(|n, n_1+1, n_2\rangle \pm |n, n_1, n_2+1\rangle)$ [7,14,15], whose frequencies are $\tilde{\omega}_{\pm} = \omega_m \pm \frac{\lambda}{2}$, respectively. In the reference frame rotating at the frequency ω_m , the frequencies of the two dressed states become $\omega_{\pm} = \pm \frac{\lambda}{2}$, which are the positions of the two transparency dips shown in Fig. 6. The two transparency windows at $\omega = \omega_{\pm}$ in Fig. 6 are the results of the destructive interferences between the incident quantized field at frequency ω_p and the quantum anti-Stokes fields at frequencies $\omega_c + \tilde{\omega}_{\pm}$ generated by the interactions of the coupling field at frequency ω_c with the two dressed states at frequencies $\tilde{\omega}_{\pm}$, respectively. The separation between the two transparency dips is $D = \omega_+ - \omega_- = \lambda$. Thus the separation D between the two transparency dips is equal to the Coulomb coupling strength λ , which is consistent with the numerical result shown in Fig. 7. It is worth mentioning

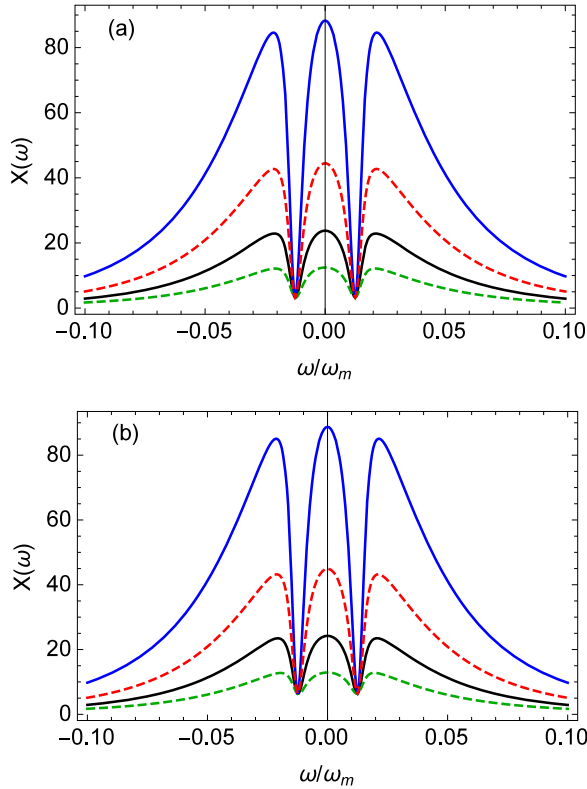


FIG. 9. Homodyne spectrum $X(\omega)$ as a function of the normalized frequency ω/ω_m for different values of the parameter N in the presence of the coupling field when $\lambda = 0.5\kappa$, $M = \sqrt{N(N+1)}$ and 0, $\wp = 20 \mu\text{W}$, and (a) $T = 10 \text{ mK}$ and (b) $T = 20 \text{ mK}$. In each plot the upper two curves are for $N = 5$ and the lower two curves are for $N = 1$; the solid curves are for $M = \sqrt{N(N+1)}$ and the dashed curves are for $M = 0$.

that the maximum value of the Coulomb coupling strength in Figs. 6 and 7 is taken to be $\lambda = \kappa = 2\pi \times 6.8 \text{ kHz}$, which is on the same order of magnitude as the Coulomb coupling strength $2\pi \times 3.1 \text{ kHz}$ between two mechanical oscillators in the experiment in [45]. Figure 9 shows the homodyne spectrum $X(\omega)$ of the output field versus the normalized frequency ω/ω_m in the presence of the coupling field for $\lambda = 0.5\kappa$, $N = 1$ and 5, $M = \sqrt{N(N+1)}$ and 0, $\wp = 20 \mu\text{W}$, and $T = 10$ and 20 mK. Let us first consider the case of $M = \sqrt{N(N+1)}$. For a given temperature T , it is seen that the double EIT dips still appear in the homodyne spectrum $X(\omega)$ for $N = 1$ and 5 and the double EIT dips for $N = 1$ and 5 almost have the same minimum values (about 3.18 for $T = 10 \text{ mK}$ and about 6.35 for $T = 20 \text{ mK}$) and the same linewidths (about $0.006\omega_m$). Comparing the curves for $\lambda = 0.5\kappa$, $N = 5$, $M = \sqrt{N(N+1)}$, and $\wp = 20 \mu\text{W}$ in Fig. 9 with those in Fig. 6, it is found that the minimum values of the double EIT dips increase with increasing temperature T due to the increase of the mechanical thermal noises. Therefore, the temperature T of the environment leads to the degradation of the double EIT behavior. Similar results can be obtained in the case of $M = 0$. For a given temperature T , when $M = 0$, the double EIT dips still exist in the homodyne spectrum $X(\omega)$ for $N = 1$ and 5 and the linewidths of the double EIT dips for $N = 1$ and 5 are almost equal (about $0.006\omega_m$), which are

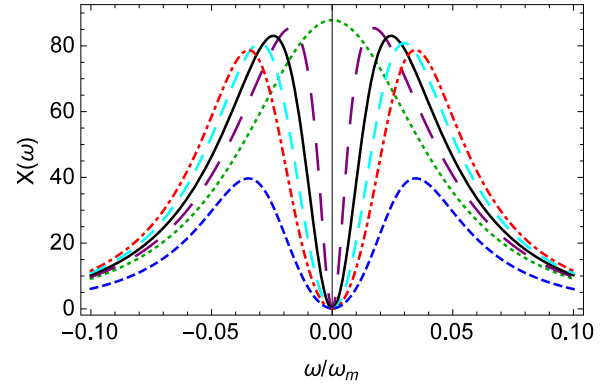


FIG. 10. Homodyne spectrum $X(\omega)$ as a function of the normalized frequency ω/ω_m in the absence (dotted curve) and presence of the coupling field with different powers when $\lambda = 0$, $N = 5$, $M = \sqrt{N(N+1)}$ and 0, and $T = 1 \text{ mK}$. The long-dashed, solid, medium-dashed, and dash-dotted curves are for $M = \sqrt{N(N+1)}$ and $\wp = 5, 10, 15$, and $20 \mu\text{W}$, respectively, and the short-dashed curve is for $M = 0$ and $\wp = 20 \mu\text{W}$.

almost the same as those in the case of $M = \sqrt{N(N+1)}$. When $T = 10 \text{ mK}$, the minimum values of the double EIT dips for $N = 1$ and 5 are about 3.22 and 3.30, respectively. When $T = 20 \text{ mK}$, the minimum values of the double EIT dips for $N = 1$ and 5 are about 6.38 and 6.47, respectively. Hence, for the fixed values of the parameters T and N , the minimum values of the double EIT dips for $M = 0$ are larger than those for $M = \sqrt{N(N+1)}$. Comparing the curves for $\lambda = 0.5\kappa$, $N = 5$, $M = 0$, and $\wp = 20 \mu\text{W}$ in Fig. 9 with those in Fig. 6, we find that the minimum values of the double EIT dips become larger for a higher temperature T . Hence, the temperature T of the environment has a negative impact on the double EIT behavior.

VI. EIT IN THE HOMODYNE SPECTRUM $X(\omega)$ IN THE PRESENCE OF COMBINED DISPERSIVE AND DISSIPATIVE COUPLING

In this section we investigate the effect of the combination of dispersive and dissipative optomechanical coupling on the EIT behavior in the homodyne spectrum $X(\omega)$ of the output field. The dispersive and dissipative coupling strengths are chosen to be $\chi = 2\pi \times 0.4\sqrt{2} \text{ Hz}$ and $g = -2\pi \times 0.1\sqrt{2} \text{ Hz}$, respectively [23].

First we consider the case without the Coulomb coupling between the two mechanical oscillators. When $\lambda = 0$ and $\wp = 20 \mu\text{W}$, the steady-state displacement q_{1s} of the mechanical oscillator MO_1 is about $-3.888 \times 10^{-13} \text{ m}$, which is very small, and thus the approximations of $\omega_0(q_1)$ and $\kappa(q_1)$ in Eq. (6) are reasonable. In Fig. 10 the homodyne spectrum $X(\omega)$ of the output field is plotted against the normalized frequency ω/ω_m in the absence and presence of the coupling field when $\lambda = 0$, $N = 5$, $M = \sqrt{N(N+1)}$ and 0, and $T = 1 \text{ mK}$. We begin with the case of $M = \sqrt{N(N+1)}$. Without the coupling field ($\wp = 0$), we observe a Lorentzian line shape in the homodyne spectrum $X(\omega)$. With the coupling field ($\wp \neq 0$), an EIT window can be observed in the homodyne spectrum $X(\omega)$. For $\wp = 5, 10, 15$, and $20 \mu\text{W}$, the linewidths

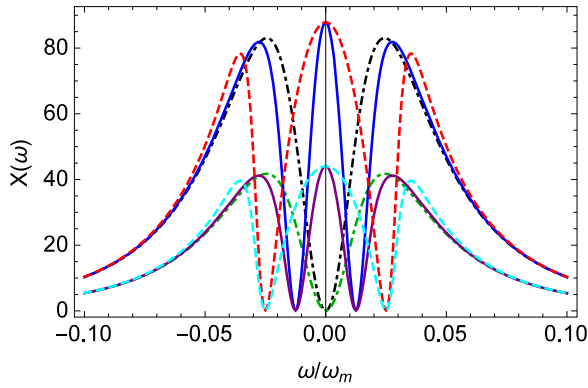


FIG. 11. Homodyne spectrum $X(\omega)$ as a function of the normalized frequency ω/ω_m for different Coulomb coupling strengths λ in the presence of the coupling field when $N = 5$, $M = \sqrt{N(N+1)}$ and 0, $\wp = 10 \mu\text{W}$, and $T = 1 \text{ mK}$. The upper three curves are for $M = \sqrt{N(N+1)}$ and the lower three curves are for $M = 0$. The dash-dotted, solid, and dashed curves represent $\lambda = 0$, 0.5κ , and κ , respectively.

of the EIT dips are about $0.011\omega_m$, $0.021\omega_m$, $0.029\omega_m$, and $0.036\omega_m$, respectively, and the minimum values of $X(\omega)$ at $\omega = 0$ are about 0.18, 0.10, 0.07, and 0.06, respectively. For $M = 0$, it is found that the minimum value of $X(\omega)$ at $\omega = 0$ for $\wp = 20 \mu\text{W}$ is about 0.15, which is larger than that for $M = \sqrt{N(N+1)}$ and $\wp = 20 \mu\text{W}$. The linewidth of the EIT dip is about $0.036\omega_m$, which is almost the same as that for $M = \sqrt{N(N+1)}$ and $\wp = 20 \mu\text{W}$. Comparing these numerical results with those obtained from Fig. 3, we find that the linewidth of the EIT dip in the case of the combined dispersive and dissipative coupling is larger than that in the case of the purely dissipative coupling, and the minimum value of the EIT dip at $\omega = 0$ in the case of the combined dispersive and dissipative coupling is less than that in the case of the purely dissipative coupling. Therefore, compared to the purely dissipative coupling case, the combined dispersive and dissipative coupling can lead to an increasing linewidth of the EIT dip and a decreasing minimum value of the EIT dip.

Next let us look at the case with the Coulomb coupling between the two mechanical oscillators. When $\lambda = \kappa$ and $\wp = 10 \mu\text{W}$, we find that the steady-state displacement q_{1s} of the mechanical oscillator MO_1 is about $-1.945 \times 10^{-13} \text{ m}$, which is very small, and thus the approximations of $\omega_0(q_1)$ and $\kappa(q_1)$ in Eq. (6) are valid. In Fig. 11 the homodyne spectrum $X(\omega)$ of the output field is plotted versus the normalized frequency ω/ω_m for different Coulomb coupling strengths λ in the presence of the coupling field when $N = 5$, $M = \sqrt{N(N+1)}$ and 0, $\wp = 10 \mu\text{W}$, and $T = 1 \text{ mK}$. For a given value of the parameter M , without the Coulomb coupling ($\lambda = 0$), only a single EIT dip is seen in the homodyne spectrum $X(\omega)$.

For a given value of M , with the Coulomb coupling ($\lambda \neq 0$), two symmetric EIT dips are observed in the homodyne spectrum $X(\omega)$. When $M = \sqrt{N(N+1)}$ or 0, the double EIT dips for $\lambda = 0.5\kappa$ and κ are located at $\omega = \pm 0.0125\omega_m$ and $\pm 0.025\omega_m$, respectively, and the linewidths of the double EIT dips for $\lambda = 0.5\kappa$ and κ are $0.0105\omega_m$ and $0.012\omega_m$, respectively. When $M = \sqrt{N(N+1)}$, the minimum values of the double EIT dips for $\lambda = 0.5\kappa$ and κ are almost the same (about 0.177). When $M = 0$, the minimum values of the double EIT dips for $\lambda = 0.5\kappa$ and κ are about 0.229 and 0.176, respectively. The comparison of these results with those for the purely dissipative coupling case shown in Fig. 6 reveals that the combined dispersive and dissipative coupling can result in an increase in the linewidths of the double EIT dips and a decrease in the minimum values of the double EIT dips.

VII. CONCLUSION

We have demonstrated the propagation of a quantized probe field in a dissipative optomechanical system with two mechanical oscillators coupled to each other through the Coulomb interaction. Without the Coulomb coupling, an EIT dip appears in the homodyne spectrum of the output field, allowing the possibility of using the dissipative optomechanical system to realize quantum memory of a squeezed vacuum. We showed that the squeezing phase of the squeezed vacuum field has an impact on the depth of the EIT dip. We found that the temperature of the environment leads to the degradation of the EIT behavior. With the Coulomb coupling, two EIT dips appear in the homodyne spectrum of the output field. We found that the distance of the double transparency windows can be used to detect the Coulomb coupling strength. The two EIT dips show that the system becomes transparent simultaneously at two different frequencies of the quantized probe field; hence such a system has potential applications in double-channel optical communication and double-channel quantum information processing [49]. In contrast to the case of the purely dissipative coupling, the combination of the dispersive and dissipative coupling can make the linewidth of the EIT dip larger and the minimum value of the EIT dip smaller.

ACKNOWLEDGMENTS

This work was supported by the National Natural Science Foundation of China under Grants No. 12174344, No. 12175199, and No. 91636108; the Zhejiang Provincial Natural Science Foundation of China under Grants No. LY21A040007 and No. LZ20A040002; and the Science Foundation of Zhejiang Sci-Tech University under Grants No. 18062121-Y and No. 17062071-Y.

[1] K.-J. Boller, A. Imamoglu, and S. E. Harris, Observation of Electromagnetically Induced Transparency, *Phys. Rev. Lett.* **66**, 2593 (1991).

[2] D. Akamatsu, K. Akiba, and M. Kozuma, Electromagnetically Induced Transparency with Squeezed Vacuum, *Phys. Rev. Lett.* **92**, 203602 (2004).

- [3] D. Akamatsu, Y. Yokoi, M. Arikawa, S. Nagatsuka, T. Tanimura, A. Furusawa, and M. Kozuma, Ultraslow Propagation of Squeezed Vacuum Pulses with Electromagnetically Induced Transparency, *Phys. Rev. Lett.* **99**, 153602 (2007).
- [4] J. Appel, E. Figueroa, D. Korystov, M. Lobino, and A. I. Lvovsky, Quantum Memory for Squeezed Light, *Phys. Rev. Lett.* **100**, 093602 (2008).
- [5] K. Honda, D. Akamatsu, M. Arikawa, Y. Yokoi, K. Akiba, S. Nagatsuka, T. Tanimura, A. Furusawa, and M. Kozuma, Storage and Retrieval of a Squeezed Vacuum, *Phys. Rev. Lett.* **100**, 093601 (2008).
- [6] G. S. Agarwal and S. Huang, Electromagnetically induced transparency in mechanical effects of light, *Phys. Rev. A* **81**, 041803(R) (2010).
- [7] S. Weis, R. Rivière, S. Deléglise, E. Gavartin, O. Arcizet, A. Schliesser, and T. J. Kippenberg, Optomechanically induced transparency, *Science* **330**, 1520 (2010).
- [8] A. H. Safavi-Naeini, T. P. Mayer Alegre, J. Chan, M. Eichenfield, M. Winger, Q. Lin, J. T. Hill, D. Chang, and O. Painter, Electromagnetically induced transparency and slow light with optomechanics, *Nature (London)* **472**, 69 (2011).
- [9] G. S. Agarwal and S. Huang, Optomechanical systems as single-photon routers, *Phys. Rev. A* **85**, 021801(R) (2012).
- [10] V. Fiore, C. Dong, M. C. Kuzyk, and H. Wang, Optomechanical light storage in a silica microresonator, *Phys. Rev. A* **87**, 023812 (2013).
- [11] J. Q. Zhang, Y. Li, M. Feng, and Y. Xu, Precision measurement of electrical charge with optomechanically induced transparency, *Phys. Rev. A* **86**, 053806 (2012).
- [12] S. Huang, Double electromagnetically induced transparency and narrowing of probe absorption in a ring cavity with nanomechanical mirrors, *J. Phys. B* **47**, 055504 (2014).
- [13] D.-G. Lai, X. Wang, W. Qin, B.-P. Hou, F. Nori, and J.-Q. Liao, Tunable optomechanically induced transparency by controlling the dark-mode effect, *Phys. Rev. A* **102**, 023707 (2020).
- [14] H. Wang, X. Gu, Y. X. Liu, A. Miranowicz, and F. Nori, Optomechanical analog of two-color electromagnetically induced transparency: Photon transmission through an optomechanical device with a two-level system, *Phys. Rev. A* **90**, 023817 (2014).
- [15] P.-C. Ma, J.-Q. Zhang, Y. Xiao, M. Feng, and Z.-M. Zhang, Tunable double optomechanically induced transparency in an optomechanical system, *Phys. Rev. A* **90**, 043825 (2014).
- [16] S. Huang and G. S. Agarwal, Electromagnetically induced transparency with quantized fields in optocavity mechanics, *Phys. Rev. A* **83**, 043826 (2011).
- [17] Q. Wang, J.-Q. Zhang, P.-C. Ma, C.-M. Yao, and M. Feng, Precision measurement of the environmental temperature by tunable double optomechanically induced transparency with a squeezed field, *Phys. Rev. A* **91**, 063827 (2015).
- [18] F. Elste, S. M. Girvin, and A. A. Clerk, Quantum Noise Interference and Backaction Cooling in Cavity Nanomechanics, *Phys. Rev. Lett.* **102**, 207209 (2009).
- [19] A. Xuereb, R. Schnabel, and K. Hammerer, Dissipative Optomechanics in a Michelson-Sagnac Interferometer, *Phys. Rev. Lett.* **107**, 213604 (2011).
- [20] S. P. Tarabrin, H. Kaufer, F. Y. Khalili, R. Schnabel, and K. Hammerer, Anomalous dynamic backaction in interferometers, *Phys. Rev. A* **88**, 023809 (2013).
- [21] T. Weiss and A. Nunnenkamp, Quantum limit of laser cooling in dispersively and dissipatively coupled optomechanical systems, *Phys. Rev. A* **88**, 023850 (2013).
- [22] A. K. Tagantsev, Dissipative-coupling-assisted laser cooling: Limitations and perspectives, *Phys. Rev. A* **102**, 043520 (2020).
- [23] A. Sawadsky, H. Kaufer, R. M. Nia, S. P. Tarabrin, F. Ya. Khalili, K. Hammerer, and R. Schnabel, Observation of Generalized Optomechanical Coupling and Cooling on Cavity Resonance, *Phys. Rev. Lett.* **114**, 043601 (2015).
- [24] R. Pennetta, S. Xie, R. Zeltner, J. Hammer, and P. St. J. Russell, Optomechanical cooling and self-stabilization of a waveguide coupled to a whispering-gallery-mode resonator, *Photon. Res.* **8**, 844 (2020).
- [25] M. Li, W. H. P. Pernice, and H. X. Tang, Reactive Cavity Optical Force on Microdisk-Coupled Nanomechanical Beam Waveguides, *Phys. Rev. Lett.* **103**, 223901 (2009).
- [26] M. Wu, A. C. Hryciw, C. Healey, D. P. Lake, H. Jayakumar, M. R. Freeman, J. P. Davis, and P. E. Barclay, Dissipative and Dispersive Optomechanics in a Nanocavity Torque Sensor, *Phys. Rev. X* **4**, 021052 (2014).
- [27] A. W. Barnard, M. Zhang, G. S. Wiederhecker, M. Lipson, and P. L. McEuen, Real-time vibrations of a carbon nanotube, *Nature (London)* **566**, 89 (2019).
- [28] R. M. Cole, G. A. Brawley, V. P. Adiga, R. D. Alba, J. M. Parpia, B. Ilic, H. G. Craighead, and W. P. Bowen, Evanescent-Field Optical Readout of Graphene Mechanical Motion at Room Temperature, *Phys. Rev. Appl.* **3**, 024004 (2015).
- [29] A. K. Tagantsev and S. A. Fedorov, Quantum-Limited Measurements Using an Optical Cavity with Modulated Intrinsic Loss, *Phys. Rev. Lett.* **123**, 043602 (2019).
- [30] A. Karpenko and S. P. Vyatchanin, Dissipative coupling, dispersive coupling, and their combination in cavityless optomechanical systems, *Phys. Rev. A* **102**, 023513 (2020).
- [31] A. Karpenko and S. P. Vyatchanin, Combination of dissipative and dispersive coupling in the cavity optomechanical systems, *Phys. Rev. A* **105**, 063506 (2022).
- [32] K. Qu and G. S. Agarwal, Generating quadrature squeezed light with dissipative optomechanical coupling, *Phys. Rev. A* **91**, 063815 (2015).
- [33] D. Kilda and A. Nunnenkamp, Squeezed light and correlated photons from dissipatively coupled optomechanical systems, *J. Opt.* **18**, 014007 (2016).
- [34] A. K. Tagantsev, I. V. Sokolov, and E. S. Polzik, Dissipative versus dispersive coupling in quantum optomechanics: Squeezing ability and stability, *Phys. Rev. A* **97**, 063820 (2018).
- [35] S. Huang and G. S. Agarwal, Reactive coupling can beat the motional quantum limit of nanowaveguides coupled to a microdisk resonator, *Phys. Rev. A* **82**, 033811 (2010).
- [36] S. Huang and A. Chen, Mechanical squeezing in a dissipative optomechanical system with an optical parametric amplifier, *Phys. Rev. A* **102**, 023503 (2020).
- [37] S. Huang and A. Chen, Mechanical squeezing in a dissipative optomechanical system with two driving tones, *Phys. Rev. A* **103**, 023501 (2021).
- [38] S. Huang and G. S. Agarwal, Reactive-coupling-induced normal mode splittings in microdisk resonators coupled to waveguides, *Phys. Rev. A* **81**, 053810 (2010).
- [39] T. Weiss, C. Bruder, and A. Nunnenkamp, Strong-coupling effects in dissipatively coupled optomechanical systems, *New J. Phys.* **15**, 045017 (2013).

- [40] C. W. Gardiner, Inhibition of Atomic Phase Decays by Squeezed Light: A Direct Effect of Squeezing, *Phys. Rev. Lett.* **56**, 1917 (1986).
- [41] Z. Ficek and P. D. Drummond, Three-level atom in a broadband squeezed vacuum field. I. General theory, *Phys. Rev. A* **43**, 6247 (1991).
- [42] K. Jähne, C. Genes, K. Hammerer, M. Wallquist, E. S. Polzik, and P. Zoller, Cavity-assisted squeezing of a mechanical oscillator, *Phys. Rev. A* **79**, 063819 (2009).
- [43] J. B. Clark, F. Lecocq, R. W. Simmonds, J. Aumentado, and J. D. Teufel, Sideband cooling beyond the quantum backaction limit with squeezed light, *Nature (London)* **541**, 191 (2017).
- [44] W. K. Hensinger, D. W. Utami, H. S. Goan, K. Schwab, C. Monroe, and G. J. Milburn, Ion trap transducers for quantum electromechanical oscillators, *Phys. Rev. A* **72**, 041405(R) (2005).
- [45] K. R. Brown, C. Ospelkaus, Y. Colombe, A. C. Wilson, D. Leibfried, and D. J. Wineland, Coupled quantized mechanical oscillators, *Nature (London)* **471**, 196 (2011).
- [46] D. F. Walls and G. J. Milburn, *Quantum Optics* (Springer, Berlin, 1998).
- [47] H. Vahlbruch, M. Mehmet, K. Danzmann, and R. Schnabel, Detection of 15 dB Squeezed States of Light and their Application for the Absolute Calibration of Photoelectric Quantum Efficiency, *Phys. Rev. Lett.* **117**, 110801 (2016).
- [48] H. Zu, W. Dai, and A. T. A. M. de Waele, Development of dilution refrigerators—A review, *Cryogenics* **121**, 103390 (2022).
- [49] B. Wang, Y. Han, J. Xiao, X. Yang, C. Xie, H. Wang, and M. Xiao, Multi-dark-state resonances in cold multi-Zeeman-sublevel atoms, *Opt. Lett.* **31**, 3647 (2006).